ChemComm

COMMUNICATION

View Article Online
View Journal | View Issue

Cite this: *Chem. Commun.*, 2017, 53, 5028

Received 26th February 2017,
Accepted 11th April 2017

DOI: 10.1039/c7cc01463e

rsc.li/chemcomm

A facile self-templating synthesis of carbon frameworks with tailored hierarchical porosity for enhanced energy storage performance†

Jie Yang,‡[ab] Gaoran Li,‡[ac] Meidan Cai,[a] Pengju Pan,[a] Zhoupeng Li,[a] Yongzhong Bao*[a] and Zhongwei Chen*[c]

Herein, we present a facile synthesis of hierarchical carbon frameworks with microporous skeletons and interconnected meso/macropores by employing poly(vinylidene chloride-*co*-methyl acrylate)-*b*-polystyrene copolymers as precursors. The obtained porosity can be tuned over a broad range *via* well-selected block proportions of the precursor, enabling its advantageous applications in target-oriented energy storage systems.

Hierarchical porous carbon (HPC) has attracted extensive research interest due to its unique structure and high porosity, which endow it with great practical superiority in applications such as adsorption, electrocatalysis, lithium based batteries, and supercapacitors.[1,2] The porosity of HPCs, with critical nanoscale effects, is considered to be the key factor in its success in these applications. Thus, a well-defined HPC with exceptionally high specific surface area and controllable pore structure has been a long-term pursuit in the development of porous carbons.[3,4]

Various strategies have been reported for the preparation of porous carbons, including the direct pyrolysis of organic precursors, physical/chemical activation techniques, metal–organic framework (MOF) derivation and template approaches, *etc.* Among them, the template-based methods have been mainly used for the preparation of HPCs,[5–7] in which the removal of the templates is generally time-consuming, expensive, and even harmful to the environment. Several template-free methods, such as the use of alkyne-like polymer precursors,[8] phase separation,[9] and self-assembly strategies,[10,11] have been put forward to overcome these shortages. However, it still remains a great challenge to combine the well-controlled porosity with the facile fabrication for HPCs.

Poly(vinylidene chloride) (PVDC) is an attractive precursor to prepare porous carbon through a simple pyrolysis process.[12,13] However, the monotony of the microporous structure in the PVDC-derived carbon severely restricts its application in extended fields. Herein, we present a facile one-step route to synthesize HPCs consisting of microporous carbon skeletons and interconnected meso/macropores by employing poly(vinylidene chloride-*co*-methyl acrylate)-*b*-polystyrene (PVDC-*b*-PS) copolymers as precursors. During pyrolysis, a robust carbon framework is formed before the pyrolysis of the PS block, which facilitates the final formation of the interconnected structure. The BET surface area, pore ratio, and pore volume can be tailored over a broad range by varying the composition of the block copolymer. The well-defined HPCs derived from the PVDC-*b*-PS precursors were applied in electrical double layer capacitors (EDLCs) as well as in lithium–sulfur (Li–S) batteries to meet their specific demands for the improved performances, *e.g.*, high capacity, good rate capability, and prolonged lifespan. This strategy opens a new avenue for the design and construction of highly porous and well-defined nanostructured carbon materials for the challenging energy issues.

As illustrated in Fig. 1, PVDC-*b*-PS copolymers were synthesized *via* a surfactant-free *ab initio* RAFT emulsion polymerization strategy by using the amphiphilic poly(acrylic acid-*b*-styrene)

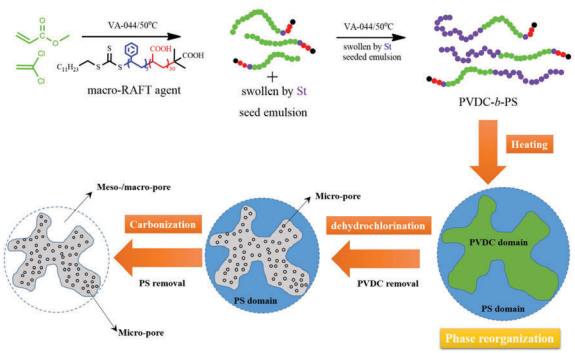

Fig. 1 Schematic illustration of the self-templating strategy for the synthesis of PVDC-*b*-PS derived HPCs.

[a] *College of Chemical and Biological Engineering, Zhejiang University, Hangzhou 310027, China. E-mail: yongzhongbao@zju.edu.cn*
[b] *Wanhua Chemical Co., Ltd. Yantai, China*
[c] *Department of Chemical Engineering, Waterloo Institute for Nanotechnology, University of Waterloo, Canada. E-mail: zhwchen@uwaterloo.ca*

† Electronic supplementary information (ESI) available: Experimental details, tables and figures. See DOI: 10.1039/c7cc01463e

‡ Jie Yang and Gaoran Li contributed equally to this work.

copolymer as a macro-RAFT agent. By varying the mass ratio between living PVDC and styrene added in the second step of the polymerization, well-defined PVDC-*b*-PS copolymers were prepared *via* a seeded emulsion polymerization process (see ESI,† Fig. S1). The copolymers with 5, 25, 52, 70 and 74 wt% of PS are denoted as PVDC-PS5, PVDC-PS25, PVDC-PS52, PVDC-PS70 and PVDC-PS74, respectively. The obtained copolymers exhibit much higher molecular weights and lower polydispersity than those prepared using solution polymerization, which are subsequently employed as the self-templating precursors to prepare HPCs (Table S1, ESI†).[13] Owing to the polarity difference between the PS and PVDC blocks, the micro-phase separated domains scaffold the carbon framework and lead to the hierarchical porous structure. For comparison, the pristine PVDC precursor was also synthesized *via* a RAFT emulsion polymerization strategy. As illustrated in Fig. S2a–e (ESI†), TEM images distinctly show that micro-fibre domains separated the features formed by the crystalline PVDC. As the content of the PVDC block gradually decreases, the morphology changes from PS-dispersed to PS/PVDC bi-continuous, and to PVDC-dispersed phase structures with 30–40 nm in domain size. The determined composition and block structure of the self-templating precursors are expected to provide well-defined and robust HPCs.

In this strategy, the PS block is regarded as a facile meso/macropore forming agent, while the PVDC block serves as a carbon source to form the micropores and carbon framework after carbonization. The step-degradation of the prepared precursors with varied the PS to PVDC ratios was confirmed *via* TGA analysis (Fig. S3, ESI†). After the subsequent degradation of PVDC (around 250 °C) and PS templates (around 450 °C), meso/macropores were formed and interconnected HPCs were successfully obtained. The XRD patterns (Fig. S4a, ESI†) and Raman spectra (Fig. S4b, ESI†) reveal the amorphous properties as well as the higher defects and disorders in the HPCs than those in PVDC.[14] The SEM images in Fig. 2 show well-defined porous morphologies with the hierarchical structure of the obtained HPCs. Randomly distributed pores are formed for HPC with 5 wt% PS block, while a more regular shape and a honeycomb-like morphology are seen at a PS block content of 25 wt%. When the content of PS is increased to above 50 wt%, the interconnected pore structure and the PVDC-derived carbon skeleton can be clearly observed, as shown in Fig. 2d–f. The microporous skeleton can be seen in the breakage (inset image) without any obvious collapses. These results indicate that the template is successfully replicated to the carbon framework, and the mesoporous structures sacrificed from the PS block are well retained.

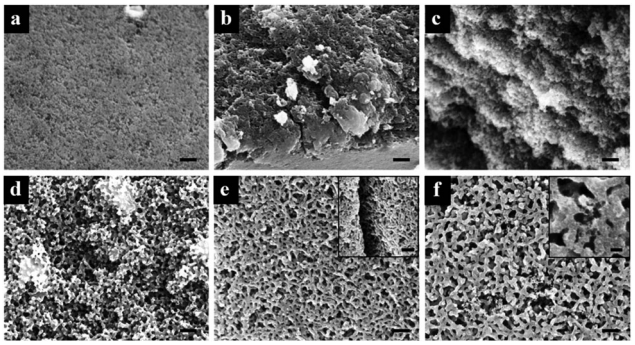

Fig. 2 SEM images of (a) PVDC-derived carbon, (b) HPC5, (c) HPC25, (d) HPC52, (e) HPC70, and (f) HPC74. The scale bars equal to 200 nm with the exception of 50 nm in the inset in (f).

Since there exist different morphologies between the precursors and the obtained HPCs, the formation mechanism of PVDC-*b*-PS derived HPCs is described as follows. The phase structure is reorganized during carbonization, then PVDC domains are merged into the microporous carbon skeleton, and finally the mesopores are attained with the removal of the PS block. The samples exhibit a pronounced increase of overall roughness as shown in AFM (Fig. S5, ESI†). The root mean square (RMS) roughness values of HPC5 and HPC74 are 3.7 and 32.5 nm after carbonization, respectively.

The removal of the PS block and the merging of the PVDC domains provide interconnected tunnels and skeletons, which are different from other carbon precursors, like phenolic resin or polyacrylonitrile. The remaining highly porous carbon framework is rigid enough to support the interconnected structure.

The porosities of the obtained HPCs were investigated through nitrogen absorption and desorption measurements (Fig. S6a, ESI†). The BET surface areas of HPC5, HPC25, HPC52, HPC70, and HPC74 are 927.8, 1239.7, 1160.1, 1225.6 and 1197.3 $m^2\ g^{-1}$ respectively (Table S2, ESI†), and the total pore volumes correspondingly increase along with the increase of the PS content in the precursor from 0.78 to 1.95 $cm^3\ g^{-1}$ (Fig. S6b, ESI†). The high pore volume combined with high surface area obtained in this work is superior to those of other PVDC-based HPCs.[13,15–17] As shown in Fig. S6c (ESI†), the pore-size distributions, calculated based on a DFT method, reveal that the HPCs mainly consist of micropores with the mean size of about 0.6 nm and a broad mesopore size distribution. It is noteworthy that the variation of the micropore size distribution is not obvious with the change of copolymer composition, while the mean size and size distribution of mesopores distinctly depend on the composition of block copolymers. For example, HPC5 has a narrow mesopore size distribution centred at 3.8 nm, while HPC74 is at 26.4 nm. Moreover, the V_{micro}/V_{total} ratio consistently decreases due to the pore size extension caused by PS pyrolysis as illustrated in Table S2 (ESI†). These results indicate that the structure parameters of the obtained HPCs can be adjusted by varying the composition of the PVDC-*b*-PS copolymer with reliable microporous skeletons. Combining the unique interconnected pore structure with the highly conductive carbon network, HPCs are endowed with inherently structural advantages in electron and ion transfer, offering great opportunities to boost the performances of various electrochemical systems, such as supercapacitive energy storages and Li–S batteries.

The EDLC performance is generally evaluated by a concomitant high capacitance and high rate capability for the electrode materials, which requires a demanding combination of the abundance of ion-accessible micropores, and the availability of meso/macropores to provide fast mass transport.[18–21] Hence, the

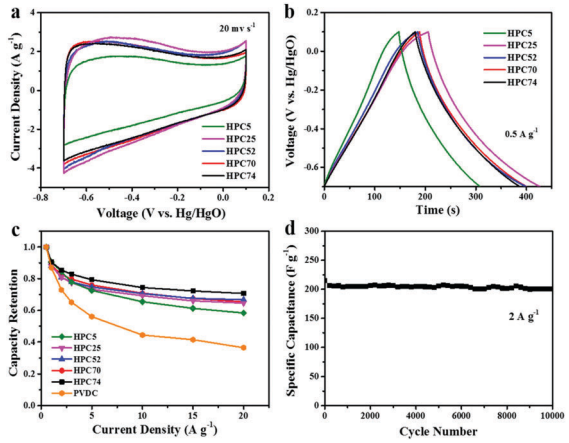

Fig. 3 Supercapacitive performances of HPCs. (a) CV curves, (b) galvanostatic curves, (c) rate capabilities of different HPC electrodes, and (d) the long-term cycling of the HPC74 electrode.

as-developed HPCs with unique multi-level pores present great potential as an active material for EDLC.

The HPC electrodes for aqueous supercapacitors were evaluated by cyclic voltammetry (CV) and galvanostatic charge–discharge (GCD) measurements. The typical approximately rectangular cyclic curves in CV and the linear shaped curves in GCD indicate the domination of the double-layer capacitance behaviour (Fig. 3a and b). The CV and GCD behaviours of different HPC electrodes are shown in Fig. S7 and S8 (ESI†). The slightly differed charge transfer impedance as shown in Fig. S9 (ESI†) may contribute to the partial asymmetry between the charge and discharge processes. The capacitances of the specimens are calculated based on GCD results. The capacitances of different electrodes at a low current of 0.5 A g^{-1} show good consistency with the BET surface areas of the prepared HPCs, as shown in Fig. 3b. The HPC5 electrode shows the smallest capacitance of 192.9 F g^{-1} due to its lowest surface area of 927.8 m^2 g^{-1}, while close capacitances of 267.1, 249.9, 250.2, and 241.9 F g^{-1} are obtained for HPC25, HPC52, HPC70, and HPC74 electrodes respectively with similarly high surface areas around 1200 m^2 g^{-1}. The high surface area enriches the electrode/electrolyte interfaces for electric double layer configurations and thereby enhances capacitances. However, these HPC electrodes exhibit very different capacity fading behaviours in rate performance, *i.e.*, those with higher pore volumes hold higher capacitance retentions under the raised current densities (Fig. 3c and Fig. S10, ESI†). The HPC74 electrode achieves the highest capacitance retention of 70.7% when increasing the current from 0.5 A g^{-1} to 20 A g^{-1}. In contrast, only 58.3% retention is obtained for the HPC5 electrode. This is ascribed to the fact that the larger pore size contributes to the improved electrolyte wettability, faster mass transfer and thereby the enhanced rate capability.[22] The rate performances of the as-prepared HPC electrodes manifest the critical role of meso/macropores over micropores in HPCs for fast charge–discharge, which can be further demonstrated by the even severer capacitance decline with a low retention of 36.3% at 20 A g^{-1} for the pure PVDC-derived specimen with dominant microporous structure.

Furthermore, a long-term cycling test was also performed for the HPC74 electrode. The result shows an outstanding cycling stability with a high capacity retention of 93.3% over an ultra-long cycle (10 000 cycles) at a current density of 2 A g^{-1} (Fig. 3d), indicating the robust integrity and the stable electrochemistry of the hierarchical carbon framework. Electrochemical evaluations performed in two-electrode configurations also show similar performance evolution among the HPC electrodes, where the HPC74 electrode still achieves the best rate capability and high cycling stability (Fig. S11, ESI†). Therefore, by tuning the composition of the precursor, the HPC with both abundant active interfaces and sufficient ion transfer paths is achieved for the combined high specific capacitance, excellent rate capacity and outstanding cycling stability.

Li–S batteries have emerged as an attractive energy storage candidate due to their inherent merits, *e.g.*, high energy density and low cost.[23,24] However, several problems, including the active material insulativity, the large volume change and the parasitic polysulfide shuttling, should be well addressed before their practical applications. The employment of porous carbon as a conductive sulfur host has exerted considerable potential in tackling these problems.[25] The as-developed HPCs with interconnected conductive frameworks and highly tunable pore structures show great potential as the specifically designed conductive substrate for the sulfur electrodes.

The HPC-based sulfur electrodes (S@HPCs) were prepared *via* conventional processes (see details in the ESI†). The galvanostatic measurements show the best cycling performance for the S@HPC70 electrode with a high initial capacity of 1299.8 mA h g^{-1} at C/5 (1C = 1675 mA h g^{-1}) and a considerable capacity retention of 892.9 mA h g^{-1} after 50 cycles (Fig. 4a). The S@HPC70 electrode also achieves the best rate capability with a reversible capacity of 540 mA h g^{-1} at a high rate even up to 10C (Fig. 4b), indicating its fast reaction kinetics and great electrochemical reversibility. In contrast, the S@HPC electrodes exhibit deteriorated cycling and rate performances along

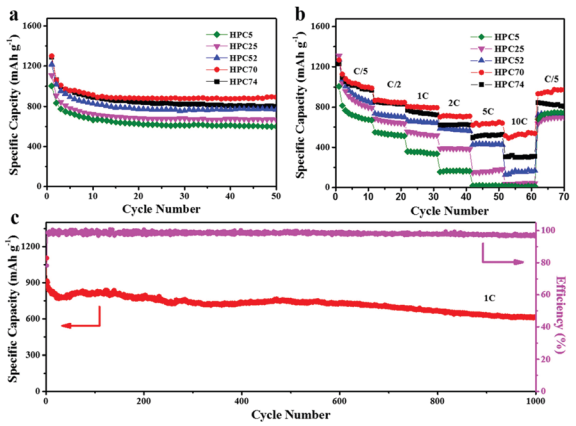

Fig. 4 Li–S battery performances. (a) Cycling performances at C/5 and (b) rate performances for different S@HPC electrodes, and (c) capacity and coulombic efficiency of the S@HPC70 electrode over 1000 cycles at 1C.

with the decrease of the PS block, while the S@HPC74 electrodes achieve relatively poorer performances than those of S@HPC70, but superior rate capability than those with a lower PS block content. These results indicate a strong dependence of the Li–S battery performances on the HPC pore structure.

As mentioned above, the pore volumes of the obtained HPCs experience a positive growth along with the increase of PS content in polymer precursors, showing a sustained increase of meso/macropore content and average pore size in HPCs. More commendably, the pore volume increase does not sacrifice the BET surface areas, which maintains at a high level during this process (Table S2, ESI†). The effect of the pore structure of HPCs on the Li–S battery performance is ascribed as follows: (a) the high surface area provides sufficient sulfur–carbon contact, leading to an improved electron transfer and enhanced sulfur utilization, which explains the lowest capacity of the S@HPC5 electrode with the smallest S_{BET}; (b) a higher pore volume is conducive to hold more sulfur inside the pores when the sulfur content is relatively high as $\sim$70 wt% in our case, so as to reduce the sulfur loss caused by polysulfide shuttling; (c) with a large pore volume, the surplus space after sulfur loading facilitates to hold the volume expansion during the lithiation process, and also an improved electrolyte wettability for sufficient ion supply. Therefore, the electrodes with larger pore volumes reveal higher capacity and improved rate capability; (d) however, an excessively large pore size also brings in negative effects by offering a larger exit for sulfur escape, which leads to a faster capacity decay of the S@HPC74 electrode compared to S@HPC70. These effects are evidentially supported by the smallest potential gap of 0.144 V in the voltage profile (Fig. S12, ESI†), the sharpest peaks and the smallest peak potential gaps in CV curves (Fig. S13a, ESI†), as well as the smallest impedance in the EIS spectrum (Fig. S13b, ESI†) for the S@HPC70 electrode with an appropriately high pore volume and a large pore size, indicating its significantly improved sulfur electrochemistry.

Based on these results, a long-term cycling test was further performed at the 1C rate for the S@HPC70 electrode as shown in Fig. 4c. A high capacity of 611.6 mA h g^{-1} and a constant coulombic efficiency above 97% are obtained over an ultra-long charge–discharge of 1000 cycles, with a negligible capacity decay of 0.033% per cycle starting from the second cycle, revealing its outstanding cycling stability. Therefore, by tailoring the porosity through this strategy, HPC70 is achieved with a great integration of the high BET surface area, an adequate pore volume, and an appropriate pore size for the sulfur electrode, thus achieving the best cycling and rate performances.

In conclusion, interconnected HPC frameworks were synthesized through a facile self-templating carbonization of PVDC-*b*-PS copolymers. Because of the polarity difference between PS and PVDC blocks, the micro-phase separated structures and the tunable composition result in interconnected frameworks. By regulating the PS block content in the precursor, a high porosity controllability for the obtained HPCs is realized to meet the specific structural demands for the improved energy storages, *e.g.* supercapacitors and lithium–sulfur batteries. Excellent electrochemical performances based on well-tailored HPCs, *i.e.*, considerable rate capability and high cycling stability over 10 000 cycles for EDLC, excellent rate response up to 10C and outstanding cyclability over 1000 cycles for Li–S batteries were achieved. Underlining the unique morphology and the highly controllable porosity, the HPCs based on this strategy are endowed with great potential in electrochemical systems, such as Li–ion batteries, Li–air batteries, electrocatalysis and so forth.

This work was supported by the National Natural Science Foundation of China (Grant no. 21176209). All authors have given approval to the final version of the manuscript.

Notes and references

1 Y. Wang, Z. Wei, Y. Nie and Y. Zhang, *J. Mater. Chem. A*, 2017, **5**, 1442–1445.
2 Y. Nie, L. Li and Z. Wei, *Chem. Soc. Rev.*, 2015, **44**, 2168–2201.
3 C. Liang, Z. Li and S. Dai, *Angew. Chem., Int. Ed.*, 2008, **47**, 3696–3717.
4 R. Wu, S. Chen, Y. Zhang, Y. Wang, Y. Nie, W. Ding, X. Qi and Z. Wei, *J. Mater. Chem. A*, 2016, **4**, 2433–2437.
5 S. Zhang, L. Chen, S. Zhou, D. Zhao and L. Wu, *Chem. Mater.*, 2010, **22**, 3433–3440.
6 Y. Zhai, Y. Dou, X. Liu, S. S. Park, C. Ha and D. Zhao, *Carbon*, 2011, **49**, 545–555.
7 J. Thomassin, A. Debuigne, C. Jérôme and C. Detrembleur, *Polymer*, 2010, **51**, 2965–2971.
8 C. Zou, D. Wu, M. Li, Q. Zeng, F. Xu, Z. Huang and R. Fu, *J. Mater. Chem.*, 2010, **20**, 731–735.
9 Y. Huang, H. Q. Cai, D. Feng, D. Gu, Y. H. Deng, B. Tu, H. T. Wang, P. A. Webley and D. Y. Zhao, *Chem. Commun.*, 2008, 2641–2643.
10 Q. Zhao, T. Fellinger, M. Antonietti and J. Yuan, *J. Mater. Chem. A*, 2013, **1**, 5113–5120.
11 W. Ding, L. Li, K. Xiong, Y. Wang, W. Li, Y. Nie, S. Chen, X. Qi and Z. Wei, *J. Am. Chem. Soc.*, 2015, **137**, 5414–5420.
12 A. Bailey and D. H. Everett, *Nature*, 1966, **211**, 1082–1083.
13 J. Yang, Y. Bao and P. Pan, *J. Mater. Sci.*, 2014, **49**, 1090–1098.
14 W. Ren, F. Li, P. Tan and H. Cheng, *Phys. Rev. B: Condens. Matter Mater. Phys.*, 2006, **73**, 115430.
15 J. Yang, Y. Bao and P. Pan, *Microporous Mesoporous Mater.*, 2014, **196**, 199–207.
16 B. Xu, F. Wu, S. Chen, G. P. Cao and Z. M. Zhou, *Colloids Surf., A*, 2008, **316**, 85–88.
17 G. C. Laredo, E. Meneses, J. Castillo, J. O. Marroquin and F. Jiménez-Cruz, *Energy Fuels*, 2008, **22**, 2641–2648.
18 P. Billemont, B. Coasne and W. G. De, *Langmuir*, 2013, **29**, 3328–3338.
19 W. Gu, N. Peters and G. Yushin, *Carbon*, 2013, **53**, 292–301.
20 Y. Fang, Y. Lv, R. Che, H. Wu, X. Zhang, D. Gu, G. Zheng and D. Zhao, *J. Am. Chem. Soc.*, 2013, **135**, 1524–1530.
21 E. G. Calvo, N. Ferrera-Lorenzo, J. A. Menendez and A. Arenillas, *Microporous Mesoporous Mater.*, 2013, **168**, 206–212.
22 B. Xu, F. Wu, D. Mu, L. Dai, G. Cao, H. Zhang, S. Chen and Y. Yang, *Int. J. Hydrogen Energy*, 2010, **35**, 632–637.
23 G. Li, M. Ling, Y. Ye, Z. Li, J. Guo, Y. Yao, J. Zhu, Z. Lin and S. Zhang, *Adv. Energy Mater.*, 2015, **5**, 1500878.
24 G. Li, W. Cai, B. Liu and Z. Li, *J. Power Sources*, 2015, **294**, 187–192.
25 F. Xu, Z. Tang, S. Huang, L. Chen, Y. Liang, W. Mai, H. Zhong, R. Fu and D. Wu, *Nat. Commun.*, 2015, **6**, 7221.